SECONDARY ORGANIC AEROSOL YIELD FROM ACETYLENE OXIDATION DURING CLOUD PROCESSING CYCLES

A Thesis

by

CASSANDRA FAYE MILAN

Submitted to the Office of Graduate and Professional Studies of
Texas A&M University
in partial fulfillment of the requirements for the degree of

MASTER OF SCIENCE

Chair of Committee,	Don Collins
Committee Members,	Renyi Zhang
	Qi Ying
Head of Department,	Ping Yang

August 2018

Major Subject: Atmospheric Sciences

ABSTRACT

Many first and second generation products from oxidation of volatile organic compounds are water soluble, allowing for participation in aqueous phase chemistry. Secondary organic aerosol formation in the aqueous phase can have a substantial contribution to the overall tropospheric aerosol concentration. This work describes results from the Multiphase Aging and Production of Particles (MAPP) chamber, a new chamber designed to allow for both gas phase and cloud chemistry research. Clouds are generated within the chamber as to mimic the adiabatic expansion of a rising air parcel in the atmosphere. The adiabatic expansion cloud formation capabilities of MAPP allows for realistic studies of secondary organic aerosol production within cloud water droplets. MAPP's FEP Teflon design is unique to current cloud chambers used to studying secondary organic aerosol growth and will help reduce wall interactions that are normally present in stainless steel chambers. Studies using the MAPP chamber were done with oxidation of acetylene by hydroxyl radicals to produce glyoxal. Glyoxal, a water soluble organic species, was found to produced significant secondary organic aerosol growth in the presence of cloud droplets.

CONTRIBUTORS AND FUNDING SOURCES

Contributors

This work was supported by a thesis committee consisting of Dr. Don Collins, advisor, and Dr. Renyi Zhang of the Department of Atmospheric Sciences and Dr. Qi Ying of the Department of Civil Engineering.

All work for the thesis was completed by the student, under the advisement of Dr. Don Collins of the Department of Atmospheric Sciences.

Funding Sources

Graduate study was supported by funding from Sandia National Laboratory.

NOMENCLATURE

MAPP	Multiphase Aging and Production of Particles
SOA	Secondary Organic Aerosol
$OH^\bullet$	Hydroxyl Radical
PM	Particulate Matter
VOCs	Volatile Organic Compounds
aqSOA	Aqueous Secondary Organic Compound
HONO	Nitrous Acid
C_2H_2	Acetylene
PTFE	Polytetrafluoroethylene
FEP	Fluorinated Ethylene Propylene
RH	Relative Humidity
DMA	Differential Mobility Analyzer
CPC	Condensation Particle Counter
APS	Aerodynamic Particle Sizer
SMPS	Scanning Mobility Particle Sizer
LCL	Lifting Condensation Level
DRH	Deliquescent Relative Humidity
LWC	Liquid Water Content
AS	Ammonium Sulfate
PS	Potassium Sulfate
CLOUD	Cosmics Leaving OUtdoor Droplets chamber

CESAM	Experimental Multiphasic Atmospheric Simulation Chamber

TABLE OF CONTENTS

LIST OF FIGURES

LIST OF TABLES

TABLE Page

1. INTRODUCTION AND LITERATURE REVIEW

This thesis describes the design of the Multiphase Aging and Production of Particles (MAPP) chamber and the first experiments resulting from its use. MAPP is a new cloud chamber designed and built by our research group in the Atmospheric Sciences Department at Texas A&M University. The MAPP chamber is designed for gas phase photochemical reaction processes and production of droplets during cloud processing cycles. The purpose of MAPP, in this study, is to provide the capability for realistic controlled studies of secondary organic aerosol yields within cloud droplets.

The experiments performed and analyzed in this work use acetylene as an organic gas precursor. Oxidation of acetylene is initiated by hydroxyl radicals within the chamber to produce glyoxal. The hydroxyl radicals is created within the chamber by photolysis of nitrous acid. The purpose of the study is to calculate aqueous secondary organic aerosol yield measurements in cloud droplets from oxidation of acetylene.

1.1 Importance of Study

Particles that are suspended in Earth's atmosphere are known as aerosols. The concentration, size, chemical composition, and origin of aerosols in the atmosphere have become properties of great interest over the last several decades. Understanding these aerosol characteristics is of vital importance due to their impact on air quality and Earth's climate.

Ambient exposure to particle matter (PM) has been linked with many different significant public health problems. Nawrot et al. (2007) found a strong linear correlation between PM exposure and mortality in Berlin, Germany, especially in the summer months. Thurston et al. (2015) also found significant association between PM exposure and mortality within the United States. PM has been associated with health impacts on infants through prenatal exposure (Teng et al., 2016). Several studies have linked childhood asthma, congenital anomalies, and low birth weight to infants who have had heavy prenatal exposure to PM (van den Hooven et al., 2012; Hsu et al., 2015; Tanner et al., 2015).

PM can have both a direct and an indirect impact on climate. Direct impacts are due to the radiative scattering and absorbing properties of particles. Indirect impacts are due to the role an aerosol has as a cloud condensation nucleus or an ice nucleus. The uncertainty of aerosol-cloud and aerosol-radiation impacts on radiative forcing is a cause of considerable error in many climate models (IPCC, 2013; Zhang et al., 2013; Kodros et al., 2015).

There are many different anthropogenic and biogenic sources that contribute to the overall chemical composition and concentration of PM within the troposphere. PM are generally categorized by their source production as either primary or secondary aerosol. Primary particles are emitted directly from their source, these types of PM include dust, sea salt, or particles given off from biomass burning. Secondary particles are typically fine mode aerosol formed in part by gas phase precursors.

Secondary organic aerosol (SOA) can make up a large portion of the total atmospheric fine particle concentration. It is formed by volatile organic compounds (VOCs) whose oxidation yields products of lower volatility, which can then undergo gas-to-particle partitioning. Gas phase production alone cannot account for the total SOA concentration in the atmosphere. Blando & Turpin (2000) explored the possibility that SOA could be formed from the oxidation of organic compounds in the aqueous phase and that these products would remain in the particle phase after evaporation of the water. Since this publication, many studies have found that the additional SOA formation in aqueous phase solutions such as aerosol water, fog, and cloud droplets can lead to a considerable amount of the total SOA production, however there is still a large uncertainty in aerosol magnitude in the atmosphere especially within the SOA contribution (Ervens et al., 2011; Spracklen et al., 2011). On average, over 70% of the earth's surface is covered by clouds (Stubenrauch et al., 2013) making the evaluation of aqueous SOA (aqSOA) yields, especially in cloud droplets, an increasingly relevant topic for further assessment (Shrivastava et al., 2017; Ervens et al., 2014).

1.2 Oxidant: Hydroxal Radical Production

Many organic compounds, such as alkenes and aromatics, form highly water-soluble products during their oxidation. The production of these water-soluble species can be an important intermediate step for aqSOA formation. There are many atmospheric species capable of initializing oxidation of VOCs. Hydroxyl radical ($OH^{\bullet}$) is a gas phase constituent that is responsible for much of the oxidation processes of organic compounds.

The production of $OH^{\bullet}$ in the atmosphere can occur through many different reactions such as photolysis of ozone, nitrous acid, and formaldehyde and reactions between alkenes and ozone (Gligorovski et al., 2015). The photolysis of nitrous acid (HONO) at wavelengths between 300 nm and 400 nm (Stutz J. et al., 2000) creates $OH^{\bullet}$ as shown in Reaction 1 (R1).

$$\mathrm{HONO} + hv \rightarrow \mathrm{NO} + \mathrm{OH}^{\bullet} \tag{R1}$$

The concentration of HONO is typically higher in urban areas, but still present in suburban and remote places. The average HONO concentration on cloud-free days, around noon, in a forested area was found by Sörgel et al. (2011) to be 30 ppt with a lifetime of around 15 minutes, whereas Volkamer et al. (2010) found a campaign average of 58 pptv in Mexico City.

Though photolysis of HONO is a dominant source of $OH^{\bullet}$ in the early morning, it can contribute significantly to the overall daytime production of $OH^{\bullet}$. Volkamer et al. (2010) found HONO to be responsible for about 12% of the total daytime average $OH^{\bullet}$ production within Mexico City. Kleffmann Jörg (2007) evaluated HONO in a laboratory setting and calculated the contribution of HONO to provide up to 56% of the primary $OH^{\bullet}$ production.

1.3 Organic Precursors

Acetylene (C_2H_2), a low-molecular-weight alkyne, is an organic compound commonly found in the atmosphere. Relatively high concentrations of C_2H_2, up to 17 ppb, can be found in urban areas due to its anthropogenic sources (Calvert et al., 2000). Yaping et al. (2007) found a global combustion source of 6.6 Tg yr^{-1} for C_2H_2, with biofuel, fossil fuel, and biomass burning being responsible for 3.3 Tg yr^{-1}, 1.7 Tg yr^{-1}, and 1.6 Tg yr^{-1} respectively.

A major sink for C_2H_2 in the atmosphere is its oxidation by $OH^{\bullet}$. Several theoretically possible pathways exist for the reaction of C_2H_2 and $OH^{\bullet}$. Galano et al. (2008) modeled reaction pathways for C_2H_2 oxidation as shown in Figure 1.1. During the study, glyoxal was found to be the only significant product formed from the reaction. Though Figure 1.1 shows several possible pathways for glyoxal formation, it was found that pathway A is the main path for the reaction. In pathway A, the oxidation of C_2H_2 by $OH^{\bullet}$ in the presence of oxygen produces glyoxal while regenerating $OH^{\bullet}$.

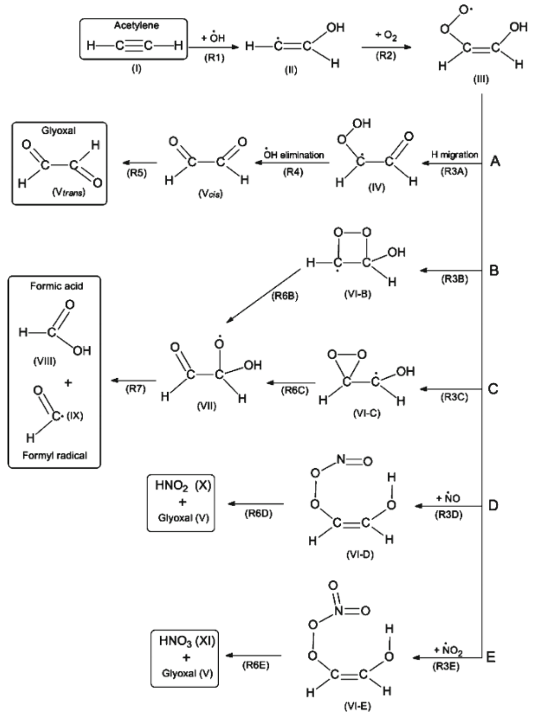

Figure 1.1: Possible reaction channels of acetylene oxidation reprinted from Galano et al., 2008

Hatakeyama et al. (1986) found oxidation of C_2H_2 to produce glyoxal with a 0.7 branching ratio. Using the branching ratio given by Hatakeyama et al. (1986), Yeung et al. (2005) found that the oxidation reaction of C_2H_2 by $OH^{\bullet}$ can lead to a glyoxal production rate of 0.05 ppb hr^{-1} and is likely to be a notable source of the daytime glyoxal production in an urban atmosphere. During a study done in Mexico City, Volkamer et al. (2007) found this reaction to be responsible for approximately 8% of the total glyoxal formation within the city.

Glyoxal has a very high Henry's law constant of $2.6x10^{-7}$ M atm^{-1} (Volkamer et al., 2009) and readily partitions into the aqueous phase. Once in the aqueous phase, glyoxal can undergo further $OH^{\bullet}$ oxidation; Ervens & Volkamer (2010) listed this aqueous phase oxidation of glyoxal by $OH^{\bullet}$ to have a reaction rate constant on the order of 10^9 $M^{-1}s^{-1}$.

Studies suggest that products of glyoxal aqueous phase chemistry can differ depending on the water media type (e.g., aerosol water, fog, cloud). This is due largely to differences in concentration of dissolved species in aerosol water and cloud droplets (Ip et al., 2009). Production of organic acids by glyoxal oxidation is found to be favored within cloud droplets while oligomerization is found to be favored within aerosol water (Lim et al., 2010; Tan et al., 2009).

Oxalic acid is one of the major organic acids produced in droplets during glyoxal oxidation by $OH^{\bullet}$. In the presence of ammonia during glyoxal oxidation within droplets, ammonium oxalate is most likely formed from oxalic acid, decreasing the resulting volatility and increasing SOA production (Ortiz-Montalvo et al., 2014).

1.4 aqSOA Yield Parameters

Several factors are thought to influence the aqSOA production within cloud droplets. Liquid water content (LWC), initial VOC to NO_x concentration ratio, time of droplet interaction, and total carbon loss rate are among the suggested influential factors. Total carbon loss rate represents the production rate of gas phase water-soluble organic compounds. The correlation between these factors and aqSOA yield in cloud droplets has been previously explored in a variety of studies.

Using a cloud parcel model, Ervens et al. (2008) performed a study to analyze the impact several different factors had on the aqSOA production from isoprene in cloud droplets. This study showed the largest yield correlation ($r^2 = 0.72$) with the initial ratio of VOC and NO_x, whereas weaker yield correlated values were associated with cloud droplet interaction time ($r^2 = 0.69$) and LWC ($r^2 = 0.55$).

He et al. (2013) used a global coupled chemistry-climate model developed by the Geophysical Fluid Dynamics Laboratory to analyze the aqSOA production factors. This study found the strongest correlation with LWC ($r^2 = 0.32$) and total carbon loss ($r^2 = 0.26$). Unlike the study by Ervens et al. (2008), He et al. (2013) found VOC to NO_x ratio to have a negative correlation coefficient ($r^2 = -0.006$).

In a study of aqSOA formation from $OH^\bullet$ initiated oxidation, Ervens et al. (2014) looked at parameters controlling both wet aerosol and cloud droplet SOA production using a chemical multiphase box model. Through these simulations, it was found that formation in cloud droplets is better characterized by drop size distributions than by LWC; Ervens et al. (2014) suggests that laboratory studies should further explore the sensitivity of aqSOA yields to such parameters.

1.5 aqSOA Study Methods

Field campaigns, wet chemistry laboratory studies, models, and chamber studies are among the different methods currently used to research aqSOA production pathways and yields. Field campaigns, such as the Southern Oxidant and Aerosol Study (Sareen et al., 2016), are advantageous in that they allow for ambient studies of aqSOA pathways; however, they have difficulty isolating specific parameters of interest and are often limited in time and location accessibility. Laboratory methods, such as bulk solution experiments and experiments using vibrating orifice aerosol generators, are useful in suggesting reaction mechanisms and quantifying some variables but often lack realistic atmospheric concentrations and conditions. Models, while they have parametric control of variables, are prone to error and need to be validated by other study methods. Chambers are another commonly used tool to study aerosol formation and are helpful in filling the gaps from the other study methods due to their ability to isolate certain variables and their ability to reproduce relevant atmospheric conditions.

There are numerous environmental chambers currently in operation that are used to study SOA formation in the gas phase (Ng et al., 2007) and smog chambers that study aqueous phase SOA only in aerosol water (Volkamer et al., 2009). The Experimental Multiphasic Atmospheric Simulation Chamber (CESAM) (Wang et al., 2011) and the Cosmics Leaving OUtdoor Droplets chamber (CLOUD) (Schnitzhofer et al., 2014) are two chambers currently equipped to study cloud droplet aqSOA growth.

The CESAM simulation chamber is located in the Interuniversitary Laboratory of Atmospheric Systems in France. The chamber design and purpose was initially described in Wang et al. (2011). Since the initial chamber description, there have been several publications describing results obtained with use of the chamber. Bregonzio-Rozier et al. (2016) used CESAM to study SOA production in cloud droplets from isoprene photooxidation. This study found significantly larger SOA yields in the presence of clouds than under photooxidation of isoprene during dry experiments. Giorio et al. (2017) used CESAM to study SOA formation during cloud production from photooxidation of both isoprene and methacrolein. This study found rapid SOA production in the presence of clouds, followed by slow aqSOA evaporation once the cloud had dissipated.

MAPP is different from CLOUD and CESAM in material, size, and cloud production approaches giving it a unique contribution to the field of research; Table 1.1 compares the primary attributes of these chambers.

Table 1.1: Comparison of cloud production chambers

Chamber	Volume	Wall Material	Cloud Formation
CESAM	4.2 m^3 vertically oriented cylinder	Stainless steel	Quick expansion of synthetic water and air mixture addition of water vapor
CLOUD	26 m^3 vertically oriented cylinder	Electropolished stainless steel	Expansion
MAPP	1.2 m^3 horizontally oriented cylinder	FEP Teflon	Adiabatic expansion

2. MAPP CHAMBER DETAILS

2.1 Design

The MAPP chamber is designed for indoor studies of aerosol growth in both the gas and aqueous phases. The chamber has a unique three-layer, cylindrical design. Figure 2.1a shows the chamber rendering design; the chamber consists of an outer vessel, a middle enclosure, and an inner reaction chamber.

The outermost layer is a vacuum resilient, stainless steel vessel with an approximate volume of 3.5 m^3. The middle enclosure is a three-fold shell constructed of perforated plastic, aluminum foil, and polytetrafluoroethylene (PTFE) gasket. The lightweight, perforated plastic gives shape to the cylindrical middle layer, the aluminum foil helps to prevent UV from escaping and degrading outer materials, and the PTFE gasket acts as a highly reflective barrier increasing the light intensity inside the reaction chamber. The inner cylindrical reaction chamber has an approximate volume of 1.2 m^3 and is constructed of nearly transparent fluorinated ethylene propylene (FEP) Teflon. The inner enclosure and reaction chamber, illuminated by a LED, can be seen in Figure 2.1b which was taken by a camera mounted on the enclosure end sheet.

The reaction chamber is oriented horizontally and supported by a port on each end. Each port rests in a bearing to allow for rotation. A sprocket is attached to one of the chamber ports and chained to a motor to produce rotation of the reaction chamber along its longitudinal axis. The motorized rotation of the chamber has a rate of approximately 7 RPM. The rotation of the chamber is performed in order to assist in particle retention within the chamber. Goldberg (1971) gives mathematical expressions and experimental evidence for longer particle retention in a rotating cylindrical drum. The acting gravitational and rotational forces on each particle provides a slow outward, orbital motion for the particles within the chamber, aiding in their retention.

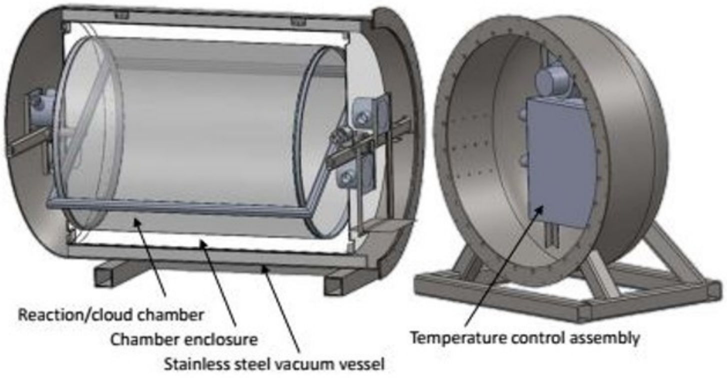

(a) Solid Works three layer design

(b) Camera image of inside the enclosure

Figure 2.1: MAPP Design

2.2 Temperature Control

Temperature is controlled by circulating air through the space between the enclosure and reaction chamber. Inside one end of the stainless-steel vessel is housed a heat exchange box. Copper tubes, which are attached to an outside reservoir of ethylene glycol and water mixture, are coiled inside of the box alongside a resistive heater. Two variable speed blowers pull warm or cool air from the box and push it through ducts to either end of the enclosure. The ethylene glycol/water mixture in the reservoir is cooled to approximately -16 ^{o}C by two chillers and pumped through the copper tubing to decrease the temperature in the chamber when needed. When warming is required, the temperature is increased by the resistive heater. Several thermistors are located between the enclosure and reaction chamber to record the temperature at different locations within the system. This system allows for temperature control of the outer walls of the reaction chamber.

2.3 Air Flow

Compressed air is initially pushed through a series of particle filters and gas filter media (activated carbon, Purafil Puracarb AM, and Purafil Chemisorbant) to inhibit contaminants from entering the chamber. The relative humidity (RH) for each experiment is regulated by controlling the amount of water vapor entering the chamber. Before entering the chamber, the chamber inlet flow is pushed through a heated container of 18.2 Milli Q (M Ω cm at 25^{o}C) water. The amount of air bubbling through the water container is managed by a bypass control valve to reach the prescribed RH set-point. The pressures inside the vessel and reaction chamber are regulated by control valves within the airflow system. A simplified diagram of the airflows to and from MAPP are shown in Figure 2.3. Polonium strips are attached inside the enclosure air ports so that the air circulating around the outside of the Teflon walls helps reduce static charge buildup.

2.4 Photolysis

A Luxtel 300 W xenon-arc lamp is mounted on the chamber enclosure. The lamp is oriented so as to radiate through a small hole in the enclosure end sheet and onto the reaction chamber. The radiation spectrum within the chamber, produced by the xenon-arc lamp, is measured using an Ocean Optics Flame Spectrometer. A fiber optic cable is attached to the enclosure and runs to the outside of the vessel where it is then attached to the spectrometer. The actinic flux is calculated from the cosine weighted irradiance measurement. The calculated actinic flux in the chamber produced by the xenon-arc lamp is shown in Figure 2.2 along with that of the solar spectrum. The two spectra taken within the chamber show two different glass filters placed over the xenon-arc lamp. Though the B270 filter resembles the solar spectrum more closely, the pyrex filter has a higher magnitude near 300 nm. As discussed in Section 1.2, the 300 nm through 400 nm wavelength range is important for the production of $OH^{\bullet}$ from HONO. For the experiments in this work, the pyrex filter was used.

It should be noted that the spectra in the chamber were taken while two xenon-arc lamps were being used. For the experiments in this work, only one xenon-arc lamp was functional. The chamber spectra shown in Figure 2.2 are reduced by 50% of the actual spectra measured in order to account for the loss of one xenon-arc lamp.

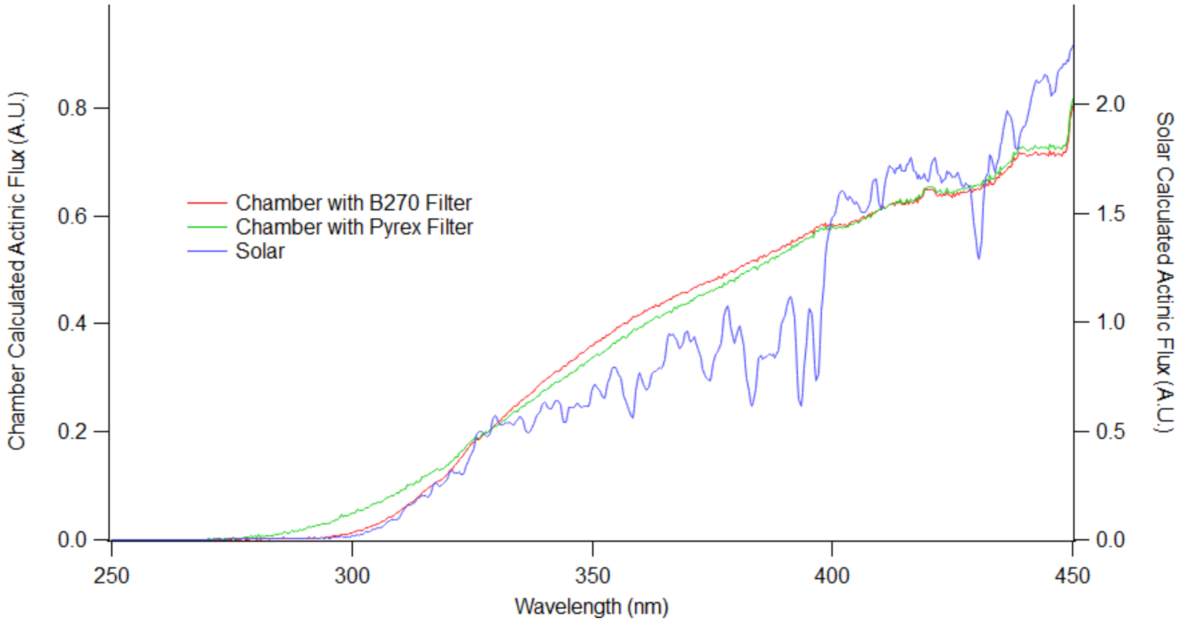

Figure 2.2: Xenon-arc lamp spectrum

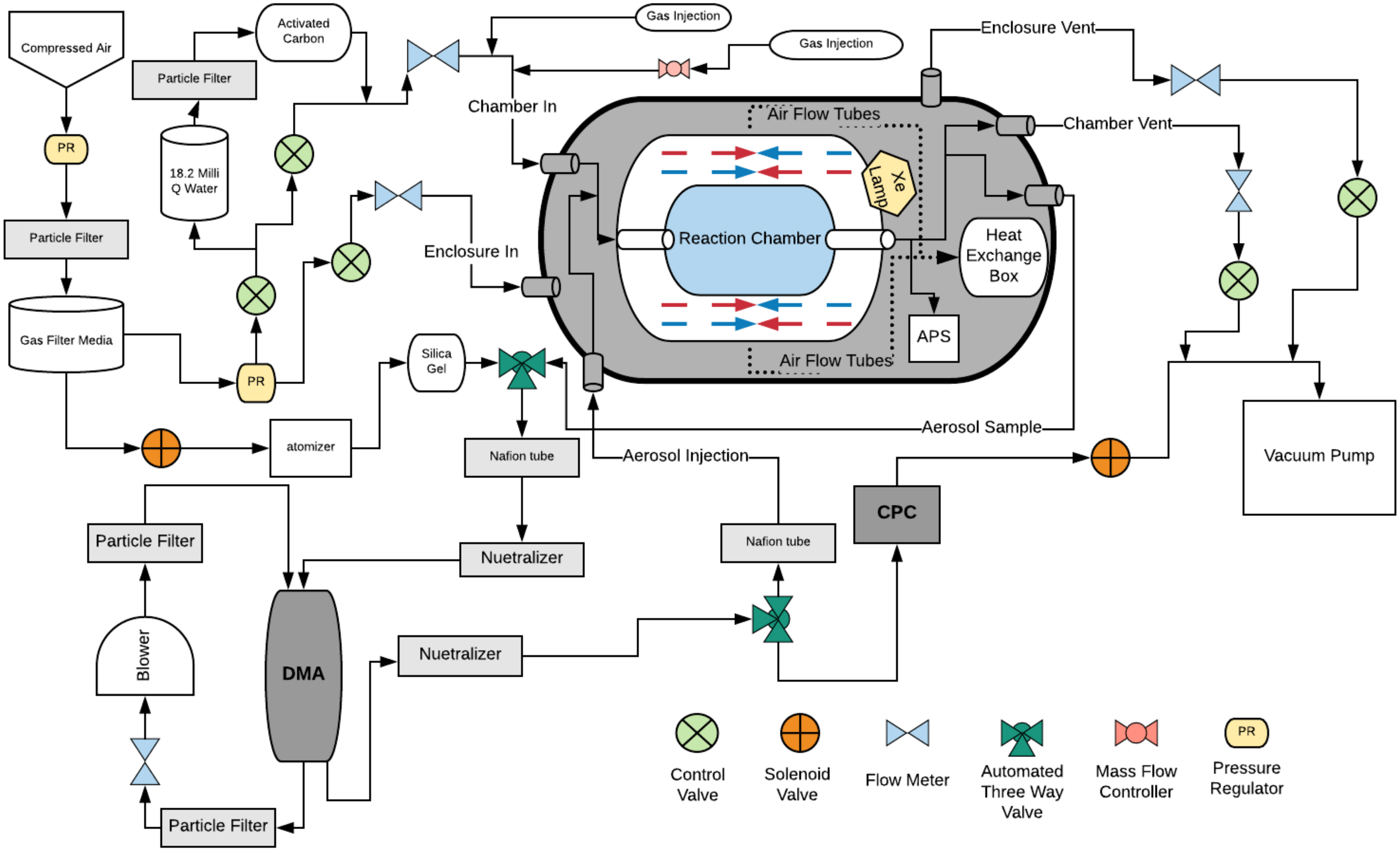

Figure 2.3: Simple flow diagram

2.5 Instrumentation

Aerosol seeds are injected into the chamber before each experiment and sampled throughout the duration of the experiment. The injected seed aerosols are formed from solution by an atomizer and dried through silica gel. The two seed aerosol types used are potassium sulfate (PS) and ammonium sulfate (AS). The particles for injection are neutralized by soft X-ray sources and dried further by a Nafion tube. A Differential Mobility Analyzer (DMA) sizes the particles for injection. A monodispersed distribution of seed particles is injected into one end of the reaction chamber through a port.

The particle mode is tracked before and after cloud formation. Samples are pulled from a chamber port through stainless steel tubing and sized by the DMA. The sized particles are detected by the Condensation Particle Counter (CPC). The DMA and CPC are operated as a Scanning Mobility Particle Sizer (SMPS). The SMPS set up is shown in Figure 2.3.

Sampling of the seed particles by the SMPS occurs leading up to cloud formation and for a time period after cloud dissipation. The sampling process is paused during cloud processing cycles due to low pressures within the chamber during cloud formation. For each sample, the DMA scan lasts approximately 6 minutes. Data gathered from the SMPS is initially retrieved as a number concentration distribution. In order to perform necessary calculations for aqSOA yields, integrated volume concentration is needed. The steps for converting from the retrieved number distribution to volume distribution are shown in equations 2.1 through 2.3.

$$\frac{\mathrm{d}V}{\mathrm{d}\log D_p} = \frac{\mathrm{d}N}{\mathrm{d}\log D_p} \times \frac{\pi}{6} \times D_p^3 \tag{2.1}$$

$$V_i = \frac{\mathrm{d}V}{\mathrm{d}\log D_p} \times \log\left(\frac{D_{i+1}}{D_i}\right) \tag{2.2}$$

$$V_{total} = \Sigma V_i \tag{2.3}$$

Figure 2.4 shows the pre- and post-cloud sampled particle measurements for both number and the corresponding calculated volume distribution for experiment 03091. In this figure, a significant change in number and volume concentration distributions can be seen between the pre- and post-cloud measurements.

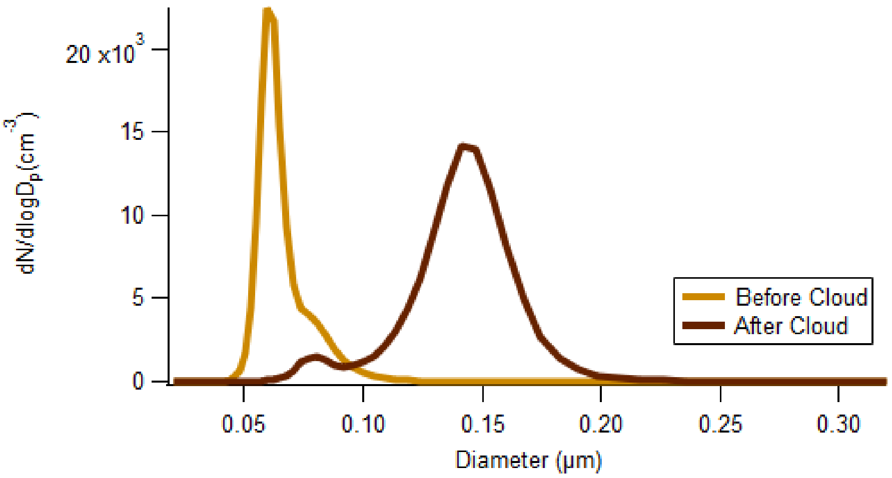

(a) Number

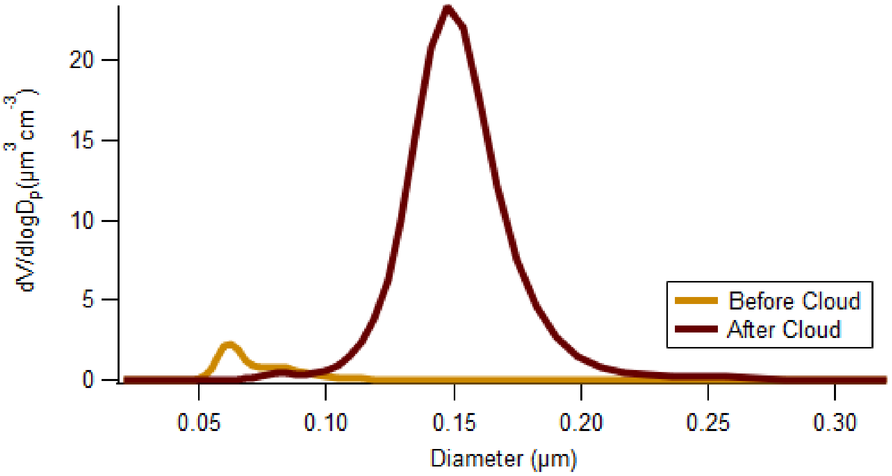

(b) Volume

Figure 2.4: Sample number and volume distributions showing before and after cloud sampled particle modes on March 9, 2018

Information on droplet size during cloud formation is gathered using a Model 3321 Aerodynamic Particle Sizer (APS). A time-of-flight particle sizing technology is used by the APS to measure the aerodynamic diameter of the droplets. The APS is situated inside of the stainless-steel vacuum vessel close to the sample port so that the length of the line leading to the APS is minimized to avoid droplet loss. The APS has a sample intake flow of about 1 liter per minute and samples continuously throughout the cloud cycle, recording 20-second averages.

2.6 Particle Retention

The loss rate of particles was measured by injecting two particle modes into the chamber and sampling the particles periodically during the experiment. The particles were held under normal experimental conditions (i.e., air circulating with blowers, chamber rotating, temperature controlled, xenon-arc lamp on). The two particle modes were sampled approximately every 30 minutes throughout a nearly 7 hour period. The peak number concentration densities for each mode during the particle retention experiment are shown in Figures 2.5a and 2.5b which denote the change in peak number concentration over the duration of the experiment. The lifetimes of a 0.05 μm and 0.15 μm particle mode were found to be 5.2 hours and 10.4 hours, respectively.

McMurry & Rader (1985) studied the loss rates for particles of different diameters and the possible influences on behavior. For particles smaller than 0.05 μm in diameter, the loss rate is heavily influenced by Brownian diffusion, the process by which fast-moving particles within a fluid cause the movement of other particles. Particles whose diameter is between 0.05 μm and 1.0 μm have a loss rate affected by electrostatic deposition, and larger particles with diameters greater than 1.0 μm are lost primarily due to gravitational sedimentation. Here, the lifetime found for a 0.05 μm injected particle mode was much less than a 0.15 μm injected mode. The more rapid loss rate of the smaller diameter mode is due to the effect that

Brownian motion has on the retention rate of the smaller diameter particles. The lifetime of the 0.15 μm injected mode is much higher than that of the smaller diameter mode and falls within the range where electrostatic deposition should be dominant. The longer lifetime of the 0.15 μm injected mode indicates that their is little, if any, electrostatic charge buildup on the walls of the FEP Teflon reaction chamber.

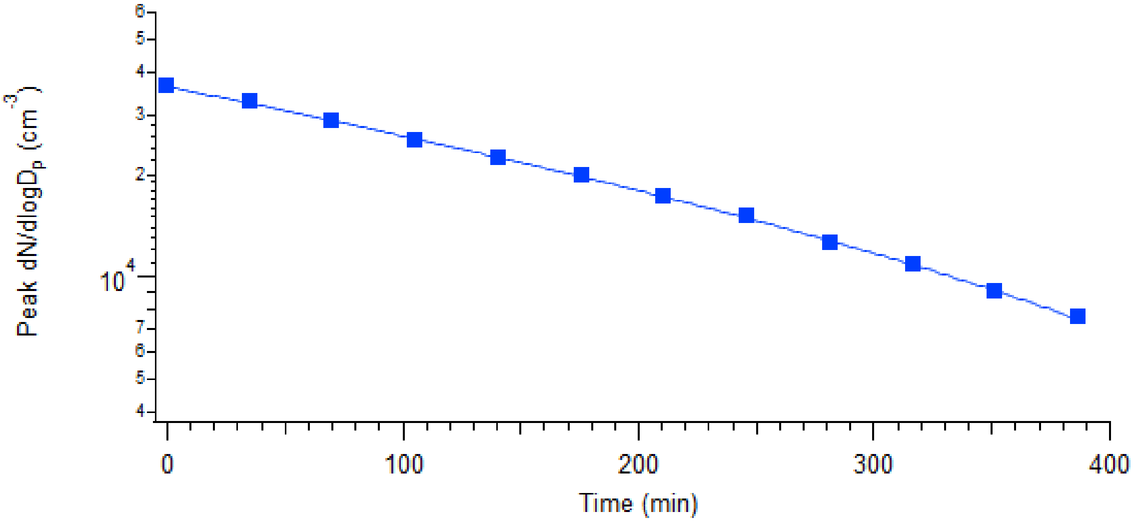

(a) 0.05 μm mode injection

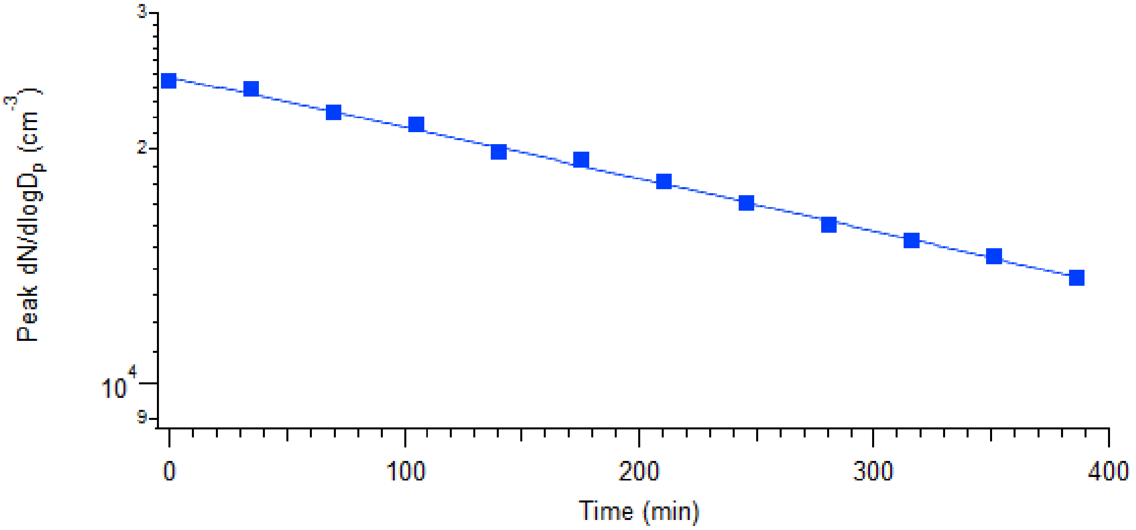

(b) 0.15 μm mode injection

Figure 2.5: Loss rate graphs of two injected particle modes

2.7 Cloud Formation

Within the reaction chamber, cloud droplets are formed through adiabatic expansion. A predetermined updraft velocity, set in the control program, determines the rate of change for the chamber pressure and temperature during a cloud cycle to realistically mimic an air parcel rising in the atmosphere. The temperature and pressure control during an experiment on March 9, 2018, with a set updraft velocity of 2.50 m s^{-1} and cloud depth of 500 meters is shown in Figure 2.6. The two lines on each of the graphs represent the program setpoint (solid line) and the measured variable (dashed line). A rotary vane vacuum pump is used to extract air, decreasing the absolute pressure within the chamber as shown in Figure 2.6a. For Figure 2.6b, the measured temperature change is an average of four temperature measurements taken at different locations on the inside of the enclosure.

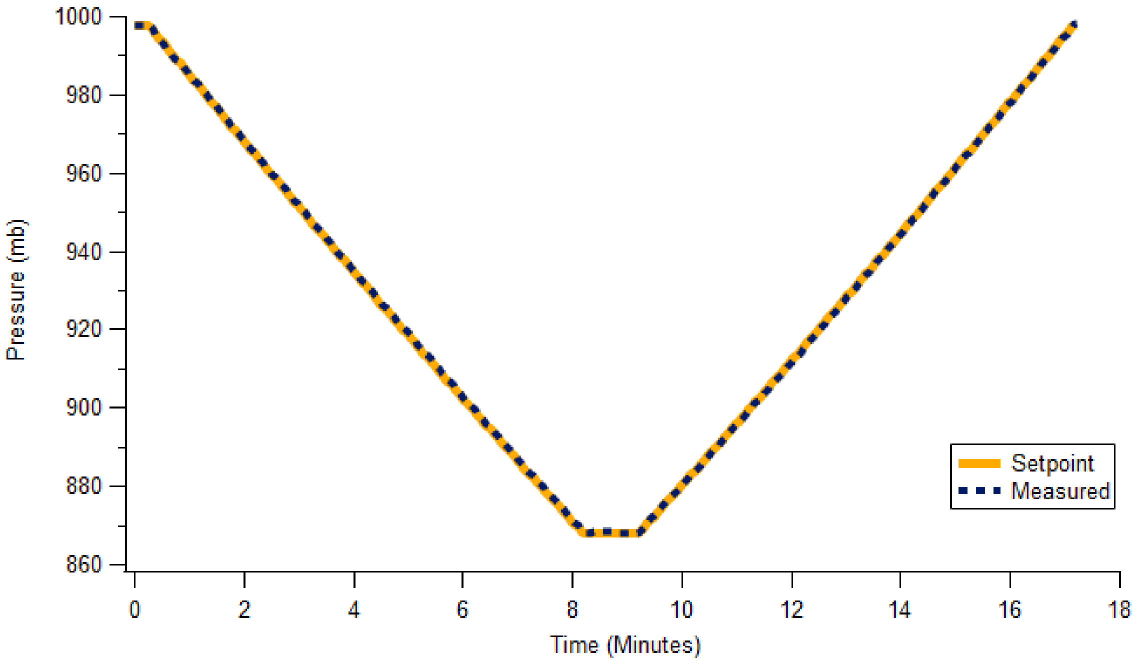

(a) Pressure profile

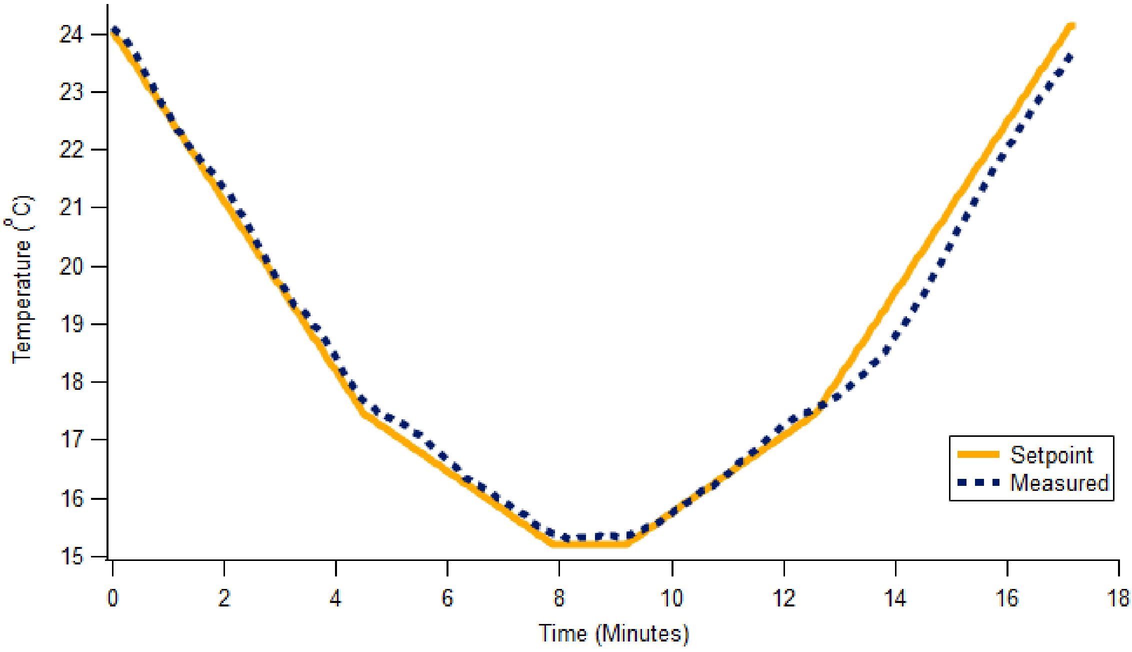

(b) Temperature profile

Figure 2.6: The measured and set point temperature and pressure profiles during a cloud cycle for experiment 03091

During the rise of an air parcel, the temperature change first follows the dry adiabatic lapse rate reaching the lifting condensation level (LCL). Cloud formation begins within the chamber when the parcel has reached the LCL. The temperature rate of change shifts at the LCL so that the parcel continues to ascend at the moist adiabatic lapse rate. This change in lapse rate can be seen experimentally in Figure 2.6b (around 17.5 ^{o}C) as the temperature slope decreases during the parcels accent.

A 540 nm sheet laser is mounted on the far end of the enclosure and pointed towards a camera on the opposite side of the chamber. During an experiment, the sheet laser illuminates the cloud droplets formed and the camera allows for sight confirmation of water droplets during predicted times within the cloud cycle. Figure 2.7 shows two pictures taken inside the reaction chamber during an experiment. The forward scattering of green light by droplets is seen only in Figure 2.7b.

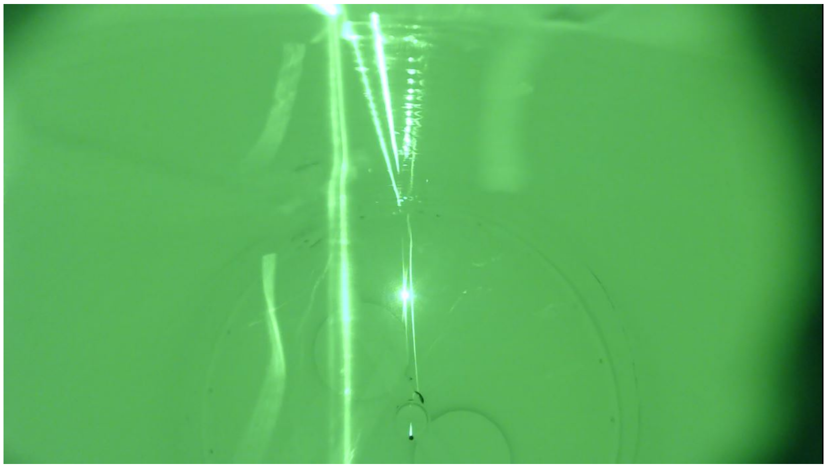

(a) Laser on before expected cloud formation

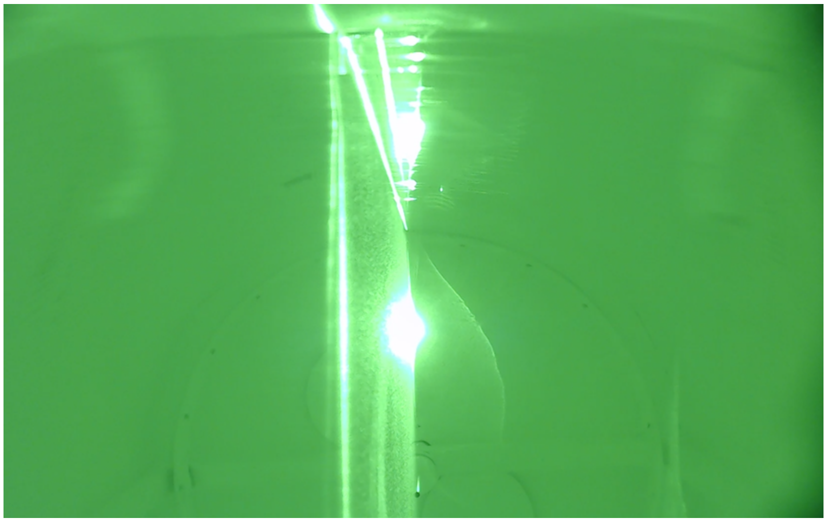

(b) laser on during expected cloud formation

Figure 2.7: Images taken inside the reaction chamber during an experiment

3. METHODS

All experiments were conducted with the MAPP reaction chamber. The chamber and enclosure were flushed overnight and before each experiment with air purified through the gas filter media and particle filters.

Ammonia, HONO, and C_2H_2 were the gas phase constituents used in each of the experiments. These gas phase species were added to the chamber through the chamber inlet flow. For the C_2H_2 injection, a pulse of gaseous C_2H_2 was added approximately one hour before cloud formation. The HONO injection was started at the same time as the C_2H_2 injection and was added continuously through the gas phase period and during cloud production. As mentioned in Section 1.3, the presence of ammonia during glyoxal oxidation in cloud droplets has been found to increase aqSOA yield. For this reason, ammonia was added to the chamber approximately twenty minutes before the cloud formation begins. The experimental time line for injections and sampling is depicted in Figure 3.1. In the figure, NH_4OH represents the injection of ammonium hydroxide.

Atomic absorption C_2H_2 (Brazos Valley Welding, 2.6 grade) was added into the chamber from a compressed cylinder. The compressed cylinder was connected to the chamber inlet flow line with Teflon tubing. The amount of injected C_2H_2 was monitored with a 100 SCCM Alicat Scientific mass flow controller. The mass flow controller was programmed to account for C_2H_2 as the measured gaseous flow.

Using a syringe, 1.5 μ L of ammonium hydroxide (EMD, 28%) was injected into a glass tube. The tube was heated to produce gaseous ammonia. A 2 liter per minute flow rate was allowed through the tube to carry the ammonia from the glass tube and into the chamber inlet flow.

HONO was produced by pumping a sodium nitrite (Alfa Aesar, 99.999%) solution drop-wise into sulfuric acid (BDH Chemicals, 0.05M). A 250 mL Pyrex round bottom flask with three top ports houses the reaction between the sulfuric acid and sodium nitrite solution. The flask was filled with approximately 150 mL of sulfuric acid. The sodium nitrite solution was pumped slowly from a syringe through one of the ports in the round bottom flask and into the sulfuric acid solution. The addition rate of the sodium nitrite solution was controlled using a Cole-Parmer programmable syringe pump. The other two ports on the round bottom flask were used to allow air to flow over the reacting solutions and into the chamber. The sulfuric acid solution was kept chilled using an ice bath to limit the amount of gaseous sulfuric acid entering the chamber.

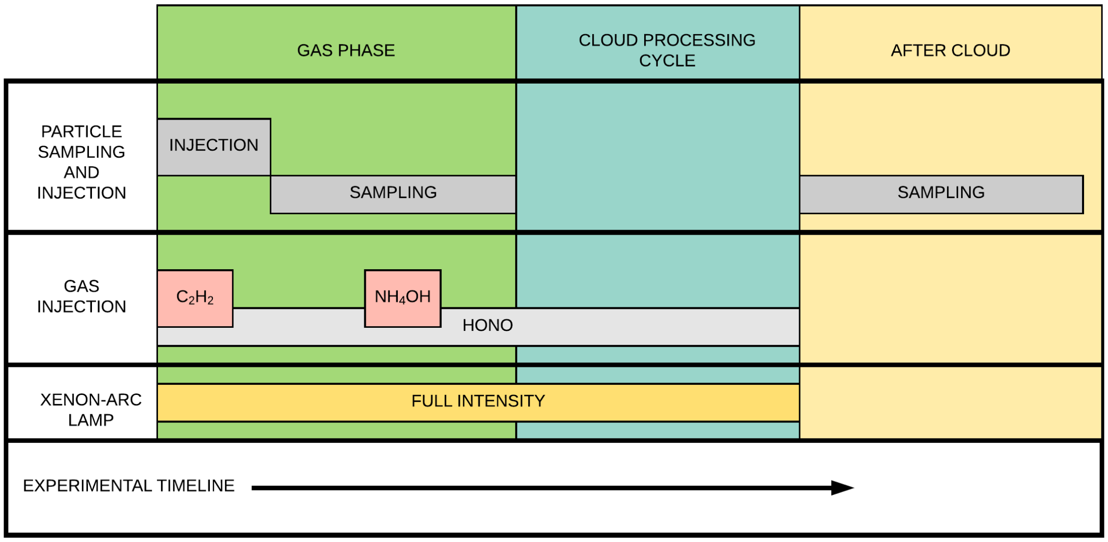

Figure 3.1: Time line for a typical experimental procedure

As discussed in Section 2.5, a seed aerosol mode was injected before each cloud cycle. The seed particles acted as cloud condensation nuclei for cloud droplet activation and provided trackable modes for aqSOA growth. PS (VWR) and AS (Mallinchrodt Chemicals) were the two seed aerosol types used in the experiments.

PS was used for the majority of the experiments due to its high deliquescent relative humidity (DRH) of 96% (Freney et al., 2009). By using a seed aerosol with a relatively high DRH, the particles should have begun to deliquesce only immediately before cloud formation, inhibiting early wet aerosol aqSOA growth. AS is a commonly used seed aerosol type in many similar studies, but due to its lower DRH of 81.7% (Brooks et al., 2002), it was not the main seed aerosol used in this study.

Before the start of each cloud cycle, the prescribed updraft velocity and cloud depth were set within the control program. For each of the experiments, the prescribed updraft velocity was set to 2.5 m s^{-1}, and the desired cloud depth was set to 500 m. The initial temperature of the chamber at the beginning of the cloud cycle ranged from 22 ^{o}C to 25 ^{o}C, and the initial RH ranged from 66% to 78%.

Table 3.1: Experiment description

Experiment	Seed Type	C_2H_2 (ppm)	[a]OH (molecules cm^{-3})	Time in gas phase (min)	[c]Cloud Lifetime (min)	Seed Volume BC ($\mu m^3 cm^{-3}$)	Δ Volume ($\mu m^3 cm^{-3}$)	Δ Mass ($\mu g\ m^{-3}$)	SOA yield (%)
[b]03151	PS	0	0	0	6.5	0.60	0.26	0.32	-
03141	PS	9	0	40	6.3	0.54	0.66	0.77	-
03071	PS	0	8.3×10^5	64	3.0	0.83	1.1	1.4	-
04201	PS	3	1.0×10^7	60	6.6	2.0	3.7	4.5	1.0
03081	PS	5	5.1×10^6	60	5.4	0.98	5.3	6.5	2.0
03091	PS	10	2.7×10^6	63	4.1	0.57	4.9	6.0	1.6
04121	PS	11	3.6×10^6	65	6.1	1.1	6.5	7.8	1.4
04191	PS	13	3.0×10^6	61	6.1	1.3	26	31	6.1
03062	PS	14	2.0×10^6	67	6.1	2.5	28	34	8.2
[b]03061	PS	14	1.9×10^6	60	4.9	0.61	3.4	4.1	1.2
04131	PS	15	2.6×10^6	60	6.0	0.97	22	27	5.4
04161	PS	18	2.4×10^6	68	6.7	0.86	27	32	5.1
04181	PS	20	2.1×10^6	64	6.2	1.4	29	35	6.7
04171	PS	21	2.2×10^6	75	5.9	1.9	69	83	11
03072	PS	24	1.3×10^6	72	6.0	0.92	67	81	17
03221	AS	23	4.2×10^6	61	5.9	1.7	24	29	2.2
03261	AS	10	8.5×10^6	64	5.9	0.75	1.0	1.3	0.094
03231	AS	14	6.6×10^6	67	6.0	1.2	14	17	1.2

[a] OH concentrations calculated at end of gas phase period, right before cloud formation.

[b] experiment preformed without NH_4OH injection.

[c] Taken from APS droplet data

4. DATA ANALYSIS

4.1 APS Data

The APS data taken during experiment 04161 is shown in Figure 4.1, along with the pressure and temperature set point profiles during the cloud processing cycle. The cloud droplets appear immediately after the set point temperature profile shifts to the moist adiabatic lapse rate. The APS data shows the duration of the cloud during an experiment based on the measurement droplets over time. The droplets, in Figure 4.1, are present in the chamber for approximately 6.7 minutes.

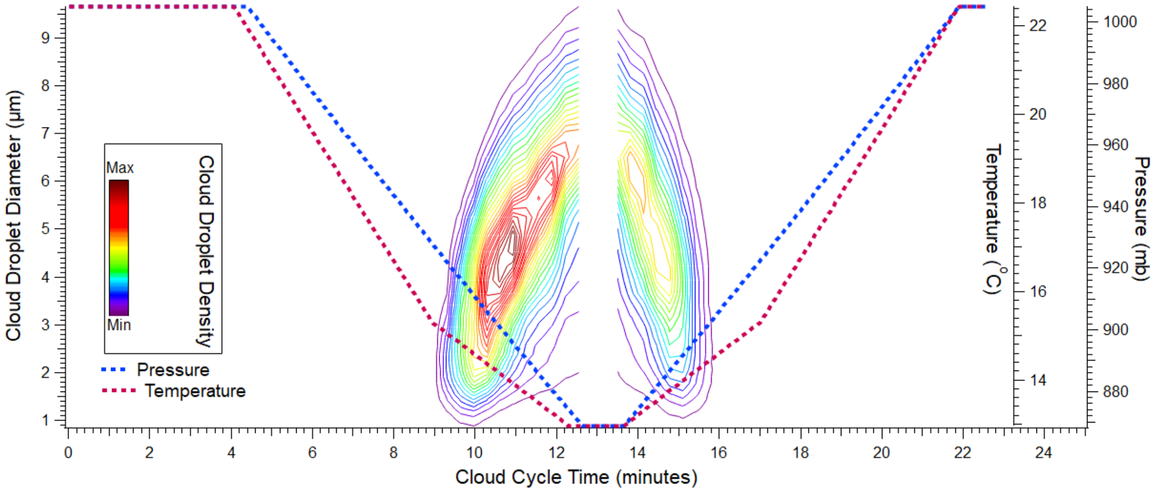

Figure 4.1: APS droplet diameter data from experiment 04161 is shown in the shaded contour plot. The pressure and temperature set points during the cloud formation are shown by the blue and red dotted lines overlaid on the contour plot.

A panel of APS data is shown for each experiment in Figures 4.2a though 4.2q. The cloud droplet size distribution during each of the experiments does show a slight variation in droplet size and distribution between each experiment. The cloud duration for each experiment was determined by the time length that droplet were present, provided by the APS data; each cloud duration is listed in Table 3.1. The average cloud duration for all experiments was found be 5.8 minutes. The peak droplet diameter that each non-blank experiment reached ranged from approximately 8 μm to 10 μm. It should be noted that the blank areas within the APS contour plots in some of the figures within the panel are time periods of missed data collection by the APS during the cloud cycle.

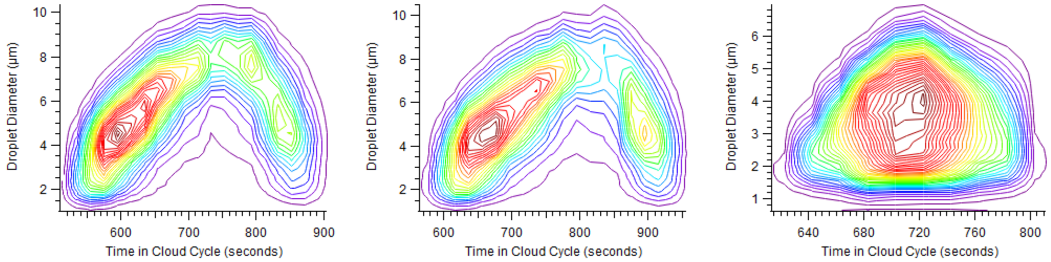

(a) Exp.03151 (b) Exp.03141 (c) Exp.03071

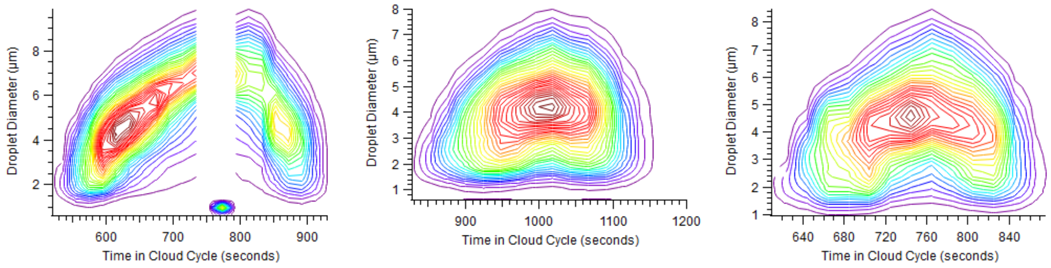

(d) Exp. 04201 (e) Exp. 03081 (f) Exp.03091

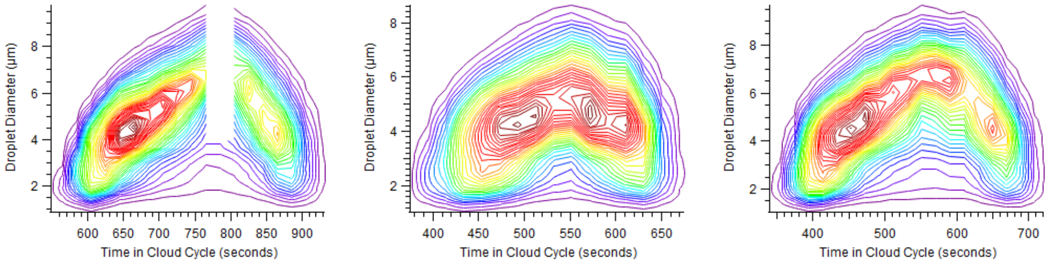

(g) Exp. 04191 (h) Exp.03061 (i) Exp.03062

Figure 4.2: APS cloud diameter data for each experiment

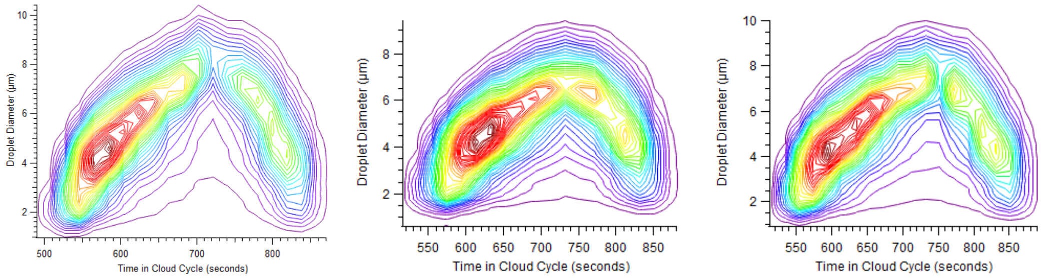

(j) Exp.04121 (k) Exp. 04131 (l) Exp. 04181

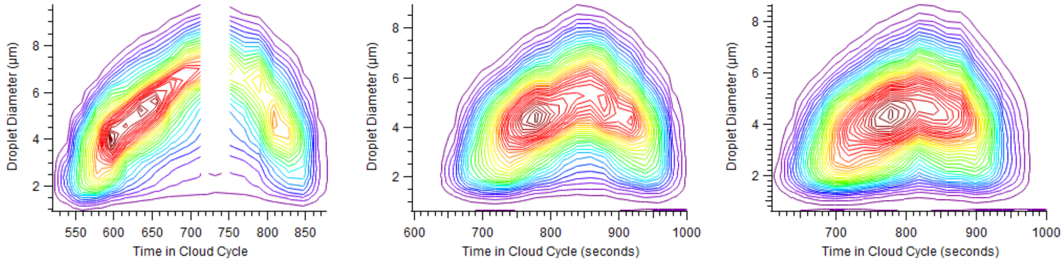

(m) Exp. 04171 (n) Exp. 03072 (o) Exp.03221

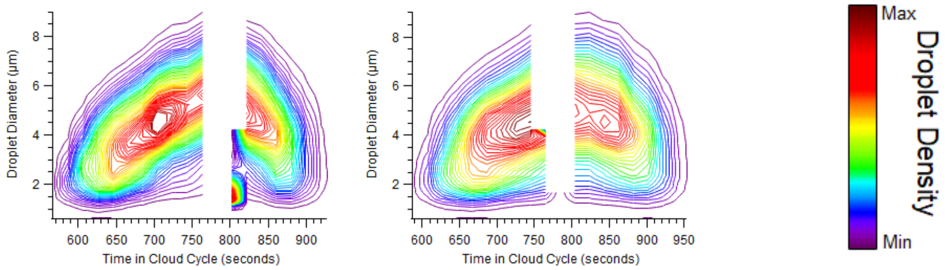

(p) Exp.03261 (q) Exp.03231

Figure 4.2: Continued

4.2 Blank Experiments

Experiments 03151, 03141, and 03071, shown in Table 3.1, were performed with some or all of the gas phase precursors absent from the experiments. These blank experiments allowed for the importance of each precursor added into the chamber to be tested. Though some of the initial gaseous precursors were missing, the xenon-arc lamp was still on at full intensity during all blank experiments.

Experiment 03151 was performed with all of the gas phase precursors absent from the experiment. Only the seed aerosol was injected before cloud formation. The small change in particle volume (0.26 μm^3 cm^{-3}) may have been due to some existing contamination within the chamber. This small change was much lower than all other experiments performed; the small amounts of growth due to contamination was relatively insignificant compared to the change in volume of non-blank experiments.

Experiment 03141 was performed without the HONO injection, the main source of OH$^\bullet$, but included a C_2H_2 injection. Experiment 03071 was performed without the C_2H_2 injection but included the HONO injection during the entire experiment. Experiment 03071 had a change in particle volume of 1.1 μm^3 cm^{-3} and 03141 had a change in particle volume of 0.66 μm^3 cm^{-3}. Both experiments showed very small volume changes during the cloud cycle. The combination of these experiments has allowed for greater confidence that growth seen in non-blank experiments was due to the expected oxidation reaction of C_2H_2 by OH$^\bullet$.

4.3 Ammonia Addition

Experiments 03061 and 03062 had similar initial conditions as shown in Table 3.1. The main difference between these two experiments was the addition of ammonium hydroxide. In experiment 03061, the introduction of ammonium hydroxide before the cloud processing cycle was absent. The aqSOA formation results between the two experiments were considerably different. The pre- and post-cloud particle volume change found after the cloud processing cycle was much greater in experiment 03062 than 03061. The 03062 had a change in particle volume of 28 μm^3 cm^{-3} and a yield of 8.2% while 03061 only had a change in particle volume of 3.4 μm^3 cm^{-3} and an SOA yield of 1.2%.

This finding was consistent with other aqSOA production measurements. Ortiz-Montalvo et al. (2014) studied the particle mass to droplet organic mass ratio after droplet evaporation. The study by Ortiz-Montalvo et al. (2014) found a significant increase of aqSOA retention in the presence of ammonium and that aqSOA retention after cloud droplet evaporation most nearly matched that of pure ammonium oxalate.

Chamber aerosol samples after cloud evaporation reveal slow particle shrinkage when samples continue for a period after cloud formation. This evaporation of particles has been observed in other aqSOA studies. Both Giorio et al. (2017) and Bregonzio-Rozier et al. (2016) attributed the slow evaporative losses to partitioning of the metastable aqSOA to the chamber wall. Shrinkage of the aqSOA particles can be calculated by equation 4.1.

$$\text{Growth Rate} = \frac{\Delta\text{peak particle diameter}}{\Delta\text{time}} \tag{4.1}$$

A solution of ammonium oxalate monohydrate (Alfa Aesar, 99.0-101.0%) was created to inject ammonium oxalate particles into the chamber. The solution was atomized, and the particles were sized by the DMA and injected into the chamber. The ammonium oxalate particle mode was held in the chamber and continuously sampled by the SMPS system for approximately an hour after injection. A graph of the number distribution for the ammonium oxalate mode over the sampling period is shown in Figure 4.3a. The ammonium oxalate particles show a considerable evaporation rate similar to that observed during after cloud sampling of experiments as shown in Figure 4.3. The calculated growth rates of the ammonium oxalate mode and experiment 04121 are -38 nm hr^{-1} and -42 nm hr^{-1} respectively.

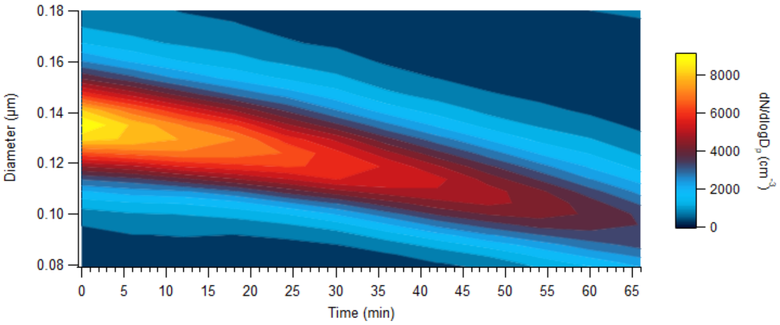

(a) Ammonium Oxalate

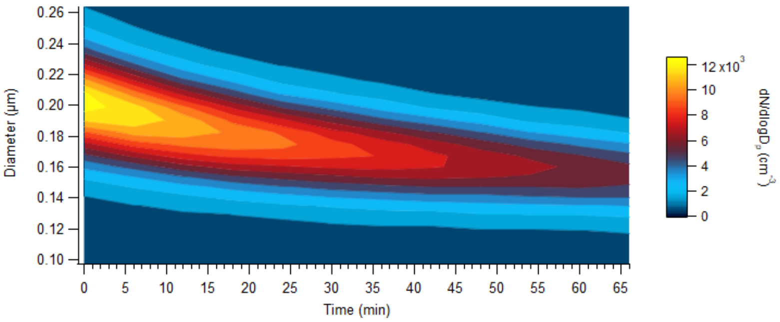

(b) Exp. 04131

Figure 4.3: After cloud sampling of evaporation rate

4.4 SOA Yield

Table 3.1 shows the change in organic mass due to aqSOA growth for each experiment; the organic mass change is calculated using the density of ammonium oxalate (1.58 g cm^{-3}). The SOA yield is calculated using the organic mass change and the mass of reacted C_2H_2. The formula for SOA yield is shown in Equation 4.2.

$$\text{SOA yield \%} = 100 \times \frac{\text{aqSOA mass}}{\text{mass of reacted } C_2H_2} \tag{4.2}$$

To determine the mass of reacted C_2H_2 during the gas phase period of each experiment, a series of gas phase reactions are taken into consideration. Table 4.1 shows the gas phase reactions expected to be taking place within the chamber. The corresponding rate constants or photolysis rates of each reaction are also listed within Table 4.1; these values are taken from previously published studies as cited within the table.

Table 4.1: Gas Phase reactions

Reaction	Reaction rate	Citation
HONO $+hv \rightarrow$ OH$^\bullet$ + NO	J$_{HONO}$=8.4×10^{-4} (s^{-1})	Alicke et al. (2003)
C_2H_2 + OH$^\bullet$ $\rightarrow$ CHOCHO + OH$^\bullet$	k$_{C_2H_2}$=1.03×10^{-12} (cm^{3}molecule^{-1}s^{-1})	Galano et al. (2008)
CHOCHO+ OH$^\bullet$$\leftrightarrow$ OCHCO + H_2O	k$_{gly}$ $= 9.15 \times 10^{-12}$ (cm^{3}molecule^{-1}s^{-1})	Feierabend et al. (2008)
CHOCHO $+hv$	$J_{gly} = 1 \times 10^{-4}$ (s^{-1})	Tadić et al. (2006)

*reactions at temperatures 296 K

*CHOCHO is glyoxal

Rate equations are derived for each of the reactions listed in Table 4.1. The rate of change for C_2H_2 is shown in Equation 4.3.

$$\frac{d[C2H2]}{dt} = -[C_2H_2][\mathrm{OH}^\bullet]k_{C_2H_2} \tag{4.3}$$

In Equation 4.4, the total rate of change for glyoxal (CHOCHO) is shown. The multiplier A represents the branching ratio of glyoxal production from the oxidation of C_2H_2. The branching ratio used within these calculations is 0.7, as found in Hatakeyama et al. (1986).

$$\begin{aligned}\frac{d[CHOCHO]}{dt} = A[C_2H_2][\mathrm{OH}^\bullet]k_{C_2H_2} - [CHOCHO][\mathrm{OH}^\bullet]k_{gly} - \\ [CHOCHO]J_{gly}\end{aligned} \tag{4.4}$$

The rate of change of HONO is shown in Equation 4.5. In the equation, the constant HONO injection source throughout the entire experiment, $[HONO]_{inj}$, is considered and depends on the drop wise addition rate used for the sodium nitrite solution.

$$\frac{d[HONO]}{dt} = [HONO]_{inj} - [HONO]J_{HONO} \tag{4.5}$$

In Equation 4.6 the rate change of $\mathrm{OH}^\bullet$ is described. The multiplier B within the equation represents the $\mathrm{OH}^\bullet$ yield from the oxidation of C_2H_2, which is 0.71 taken from Lockhart et al. (2013).

$$\begin{aligned}\frac{d[\mathrm{OH}^\bullet]}{dt} = [HONO]J_{HONO} + B[C_2H_2][\mathrm{OH}^\bullet]k_{C_2H_2} - \\ [CHOCHO][\mathrm{OH}^\bullet]k_{gly} - [C_2H_2][\mathrm{OH}^\bullet]k_{C_2H_2}\end{aligned} \tag{4.6}$$

Figure 4.4 shows an example of the chemical profiles for C_2H_2, HONO, glyoxal, and $\mathrm{OH}^\bullet$ calculated from the above rate equations for Experiment 04191. These profiles are calculated using finite differences with a time step of 0.001 seconds. The final amount of C_2H_2 reacted after the gas phase period is found by solving for the difference in initial and final C_2H_2 concentrations.

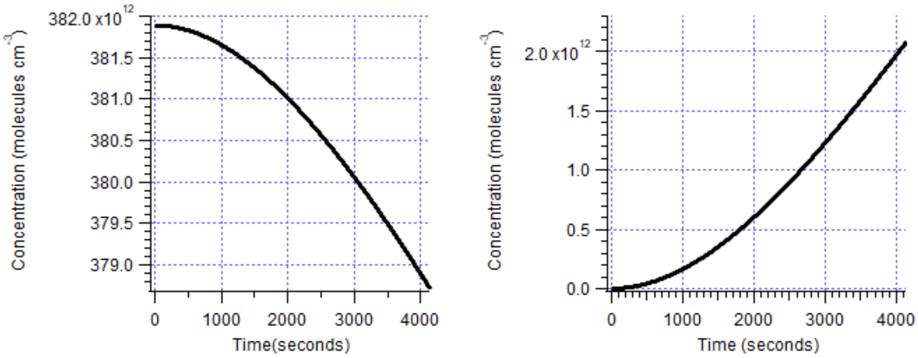

(a) C_2H_2 (b) Glyoxal

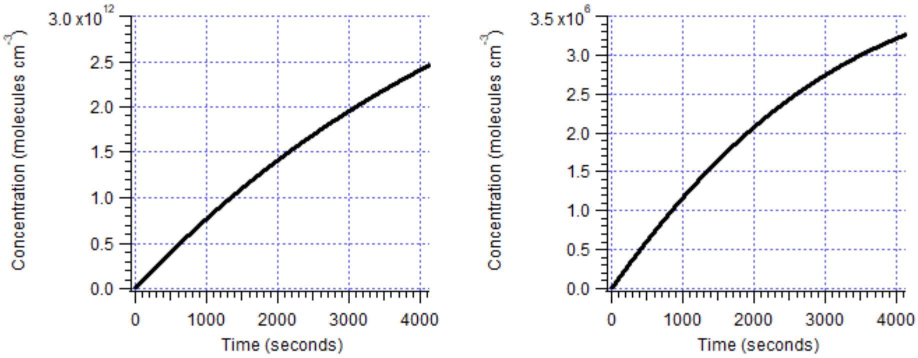

(c) HONO (d) OH

Figure 4.4: Experiment 04191 chemical profile, calculated during the gas phase period

At the end of the gas phase reaction period, the available gases may undergo aqueous phase reactions during the cloud processing cycle. The predicted aqueous phase reactions within the cloud droplets are listed in Table 4.2. These predicted reactions are taken from previously published studies as cited within the table.

Table 4.2: Aqueous Phase reactions

Reaction	Reaction rate	Citation
CHOCHO + $OH^{\bullet} \rightarrow C_2H_2O_3 +$ products	1.1×10^9 $M^{-1}s^{-1}$	Tan et al. 2009
$C_2H_2O_3 + OH^{\bullet} \rightarrow C_2H_2O_4 +$ products	2.6×10^9 $M^{-1}s^{-1}$	Carlton et al. 2007

*$C_2H_2O_3$ is glyoxylic acid

*$C_2H_2O_4$ is oxalic acid

The calculated aqSOA yields are plotted against the initial C_2H_2 injected concentration in Figure 4.5. The plot shows both the AS and PS experiments with each set of seed experiments fitted to a linear function, as shown by the dotted lines.

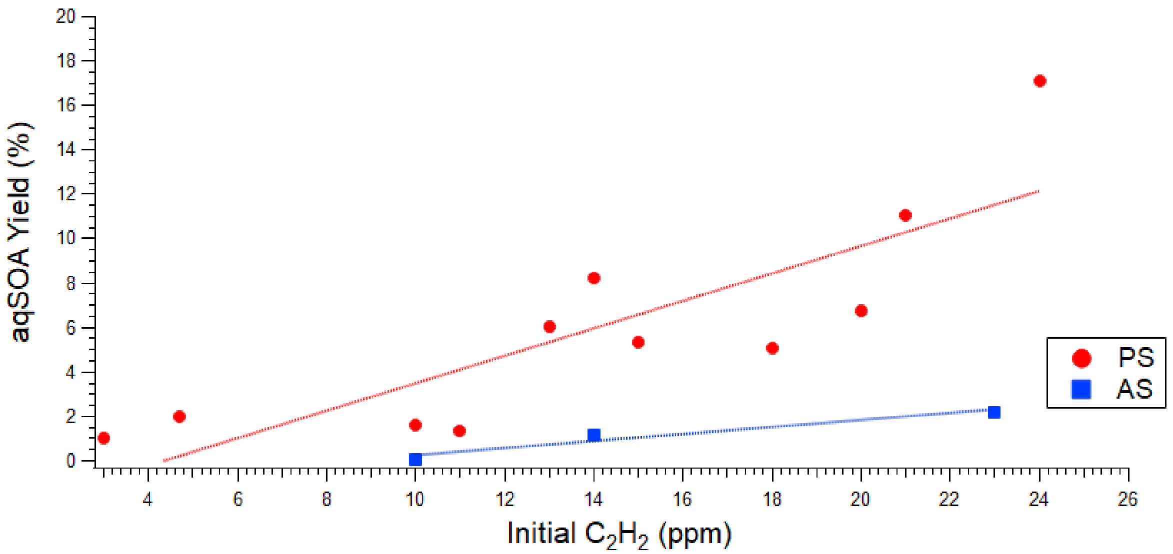

Figure 4.5: Aqueous SOA yield as a function of injected C_2H_2 concentrations. PS seed experiments (red circles) and AS seed experiments (blue squares).

The PS seed experiments show an increasing aqSOA yield with increasing initial C_2H_2

concentrations. The correlation factor for PS seed experiments is $r^2 = 0.71$. The AS seed experiments also show an increasing aqSOA yield with increasing initial C_2H_2 concentrations. The correlation factor for AS seed experiments is $r^2 = 0.94$.

The AS experiments resulted in much lower yields than the PS experiments. The lower AS aqSOA yield is consistent with the findings from Volkamer et al. (2009). Volkamer et al. (2009) compared several aqSOA yield results in aerosol water after C_2H_2 oxidation by $OH^{\bullet}$ using different types of seed aerosol, including AS seeds. They observed that AS had the lowest aqSOA yield of all the seed types.

5. SUMMARY AND CONCLUSIONS

5.1 Summary

The contribution of aqSOA formation to the overall SOA concentration in the atmosphere has been a topic of significant interest over the last few decades. A variety of studies have been conducted to find the reaction pathways, chemical composition, and concentration of aqSOA. Using chambers as a tool to study aqSOA is advantageous due to their ability to mimic atmospheric conditions and allow for control of specific variables. However, few chambers currently exist that are used to study aqSOA during cloud formation.

In response to the under-utilization of chambers in cloud aqSOA studies, the MAPP chamber was designed and built at Texas A&M University, and used perform studies that help contribute to the understanding of aqSOA production. MAPP has a multiphase functionality that allows for photooxidation of VOCs in the gas phase and produces cloud droplets for aqueous phase reactions. Using the MAPP chamber, cloud processing cycle experiments have been conducted to study aqSOA yields from oxidation of C_2H_2, an anthropologically produced organic compound.

The oxidation reaction of C_2H_2 by $OH^{\bullet}$ has been found to produce glyoxal as its only significant product, and can contribute substantially to the overall glyoxal production in a given area, especially urban environments. Glyoxal, due to its high Henry's law constant, partitions effectively into the aqueous phase and plays an important role in atmospheric aqSOA formation. A series of experiments have been performed in this work in order to quantify the aqSOA yield in cloud droplets from the oxidation of C_2H_2 by $OH^{\bullet}$.

For each experiment, precursor gases and a seed particle mode were injected and allotted a period of time for gas phase reactions followed by a cloud processing cycle. Sampling of the particle mode took place continuously leading up to the cloud processing cycle, was paused during the cycle, and continued immediately following the cloud cycle. During the cloud processing cycle, the APS ran continuously to gather data on cloud droplet diameter distribution.

The pre- and post-cloud particle number distribution was measured by the SMPS, and the corresponding change in volume distribution was calculated. The organic mass addition during a cloud cycle was found from the change in volume using the density of ammonium oxalate. The amount of C_2H_2 reacted during the experiment was calculated based on expected reactions. The aqSOA yield of each experiment was found from the change in organic mass during the cloud cycle and the mass reacted C_2H_2 during the gas phase.

5.2 Conclusions

The production of glyoxal from the oxidation of C_2H_2 by $OH^{\bullet}$ can lead to aqSOA formation in cloud droplets. Significant aqSOA growth during cloud processing cycles was found for each non-blank experiment performed within the MAPP chamber.

The addition of ammonia during the gas phase reaction period was found to have a significant impact on the formation of aqSOA. The SOA yield increased drastically in experiments with ammonium hydroxide injections. The oxidation of glyoxal within cloud droplets is predicted to form oxalic acid as its primary product. Oxalic acid is not expected to remain in the particle phase for an extended length of time due to its vapor pressure. In the presence of ammonia during the oxidation of glyoxal within cloud droplets, ammonium oxalate is predicted to form from oxalic acid. Ammonium oxalate is less volatile than oxalic acid and therefor more likely to remain in the particle phase, increasing aqSOA production.

A variety of initial C_2H_2 concentrations were used in the experiments. The blank experiments, with some of the gas phase precursors missing, showed little aqSOA growth. The lack of growth during blank experiments gives confidence that the expected gas phase reactions are responsible for the aqSOA growth seen in non-blank experiments. The non-blank experiments performed with higher initial C_2H_2 concentrations experienced higher aqSOA yields during cloud formation. A strong positive linear correlation between initial C_2H_2 concentration and aqSOA yield was found for both AS ($r^2 = 0.94$) and PS ($r^2 = 0.71$) experiments.

The difference in seed aerosol type has a considerable impact on aqSOA yield. Three AS seed particle experiments were performed using 10 ppm, 14 ppm, and 23 ppm as the initial C_2H_2 concentrations with yields of 0.12%, 1.5%, and 2.9%, respectively. The corresponding PS seed experiments with initial C_2H_2 concentrations of 10 ppm, 14 ppm, and 21 ppm experienced yields of 2.1%, 11%, and 14%, respectively. The experiments that used PS as the seed aerosol experienced much higher aqSOA yields than the experiments that used AS. The considerable aqSOA differences between PS and AS seed experiments reveals a possible large seed aerosol effect on aqSOA yields. The effect that seed aerosol has on aqSOA production should be further studied.

REFERENCES

Alicke, B., Geyer, Hofzumahaus, Holland, Konrad, Patz, … Platt (2003). Oh formation by hono photolysis during the berlioz experiment. *Journal of Geophysical Research: Atmospheres*, *108*(D4).

Blando, J., & Turpin, B. (2000). Secondary organic aerosol formation in cloud and fog droplets: a literature evaluation of plausibilty. *Atmospheric Environment*, *34*(10), 1623–1632.

Bregonzio-Rozier, L., Giorio, C., Siekmann, F., Pangui, E., Morales, S. B., Temime-Roussel, B., … Doussin, J.-F. (2016, February). Secondary organic aerosol formation from isoprene photooxidation during cloud condensation-evaporation cycles. *Atmos. Chem. Phys.*, *16*(3), 1747–1760.

Brooks, S. D., Wise, M. E., Cushing, M., & Tolbert, M. A. (2002). Deliquescence behavior of organic/ammonium sulfate aerosol. *Geophysical Research Letters*, *29*(19), 23-1-23-4.

Calvert, J., Atkinson, R., Kerr, J., Madronich, S., Moortgat, G., Wallington, J., & Yarwood, G. (2000). *The Mechanisms of Atmospheric Oxidation of the Alkenes Chap I Importance of Alkenes in the Chemistry of Ozone Generation in the Urban Atmosphere*. Oxford University Press: New York.

Carlton, A. M., Turpin, J., Altieri, B., Seitzinger, K., Reff, S., Lim, A., & Ervens, B. (2007). Atmospheric oxalic acid and soa production from glyoxal: Results of aqueous photooxidation experiments. *Atmospheric Environment*, *41*.

Ervens, B., Carlton, A. G., Turpin, B. J., Altieri, K. E., Kreidenweis, S. M., & Feingold, G. (2008). Secondary organic aerosol yields from cloud-processing of isoprene oxidation products. *Geophysical Research Letters*, *35*(2).

Ervens, B., Sorooshian, A., Lim, Y. B., & Turpin, B. J. (2014). Key parameters controlling oh-initiated formation of secondary organic aerosol in the aqueous phase (aqsoa). *Journal of Geophysical Research: Atmospheres*, *119*(7), 3997-4016.

Ervens, B., Turpin, B., & Weber, R. (2011). Secondary organic aerosol formation in cloud droplets and aqueous particles (aqsoa): a review of laboratory, field and model studies. *Atmos. Chem. Phys.*, *11*, 11069–11102.

Ervens, B., & Volkamer, R. (2010). Glyoxal processing by aerosol multiphase chemistry: towards a kinetic modeling framework of secondary organic aerosol formation in aqueous particles. *Atmospheric Chemistry and Physics*, *10*(17), 8219–8244.

Feierabend, K. J., Zhu, L., Talukdar, R. K., & Burkholder, J. (2008). Rate coefficients for the oh + hc(o)c(o)h (glyoxal) reaction between 210 and 390 k. *The Journal of Physical Chemistry*, *112*, 73-82.

Freney, E. J., Martin, S. T., & Buseck, P. R. (2009, July). Deliquescence and Efflorescence of Potassium Salts Relevant to Biomass-Burning Aerosol Particles. *Aerosol Science and Technology*, *43*(8), 799–807.

Galano, A., Ruiz-Suarez, L. G., & Vivier-Bunge, A. (2008, December). On the mechanism of the OH initiated oxidation of acetylene in the presence of O2 and NOx. *Theoretical Chemistry Accounts*, *121*(5), 219–225.

Giorio, C., Monod, A., Bregonzio-Rozier, L., DeWitt, H. L., Cazaunau, M., Temime-Roussel, B., … Doussin, J.-F. (2017, October). Cloud Processing of Secondary Organic Aerosol from Isoprene and Methacrolein Photooxidation. *J. Phys. Chem. A*, *121*(40), 7641–7654.

Gligorovski, S., Strekowski, R., Barbati, S., & Vione, D. (2015, December). Environmental Implications of Hydroxyl Radicals ($^{\bullet}$OH). *Chem. Rev.*, *115*(24), 13051–13092.

Goldberg, L. J. (1971). Naval biomedical research laboratory, programmed environment, aerosol facility. *Applied Microbiology*, *21*(2), 244-252.

Hatakeyama, S., Washida, N., & Akimato, H. (1986). Rate constants and mechanisms for the reaction of oh (od) radicals with acetylene, propyne, and 2-butyne in air at 297 +/-2 k. *Journal Phys Chem*, *90*.

He, C., Liu, J., Carlton, A. G., Fan, S., Horowitz, L. W., Levy II, H., & Tao, S. (2013). Evaluation of factors controlling global secondary organic aerosol production from cloud processes. *Atmospheric Chemistry and Physics*, *13*(4), 1913–1926.

Hsu, H.-H. L., Chiu, Y.-H. M., Coull, B. A., Kloog, I., Schwartz, J., Lee, A., … Wright, R. J. (2015). Prenatal Particulate Air Pollution and Asthma Onset in Urban Children. Identifying Sensitive Windows and Sex Differences. *American Journal of Respiratory and Critical Care Medicine*, *192*(9), 1052–1059.

Ip, H., Huang, X. H. H., & Yu, J. (2009). Effective henry's law constants of glyoxal, glyoxylic acid, and glycolic acid. *Geophysical Research Letters*, *36*.

IPCC. (2013). Summary for Policymakers. In T. Stocker et al. (Eds.), *Climate Change 2013: The Physical Science Basis. Contribution of Working Group I to the Fifth Assessment Report of the Intergovernmental Panel on Climate Change* (pp. 1–30). Cambridge, United Kingdom and New York, NY, USA: Cambridge University Press.

Kleffmann Jörg. (2007, April). Daytime Sources of Nitrous Acid (HONO) in the Atmospheric Boundary Layer. *Chem. Phys. Chem*, *8*(8), 1137–1144.

Kodros, J. K., Scott, C. E., Farina, S. C., Lee, Y. H., L'Orange, C., Volckens, J., & Pierce, J. R. (2015). Uncertainties in global aerosols and climate effects due to biofuel emissions. *Atmospheric Chemistry and Physics*, *15*(15), 8577–8596.

Lim, Y., Tan, Y., Perri, J., Seitzinger, & Turpin, B. (2010). Aqueous chemistry and its role in secondary organic aerosol (soa) formation. *Atmos. Chem. Phys.*, *10*.

Lockhart, J., Blitz, M. A., Heard, D. E., Seakins, P. W., & Shannon, R. J. (2013). Mechanism of the reaction of oh with alkynes in the presence of oxygen. *The Journal of Physical Chemistry*, *117*.

McMurry, P. H., & Rader, D. J. (1985). Aerosol wall losses in electrically charged chambers. *Aerosol Science and Technology*, *4:3*.

Nawrot, T. S., Torfs, R., Fierens, F., De Henauw, S., Hoet, P. H., Van Kersschaever, G., … Nemery, B. (2007, February). Stronger associations between daily mortality and fine particulate air pollution in summer than in winter: evidence from a heavily polluted region in western Europe. *Journal of Epidemiology and Community Health*, *61*(2), 146–149.

Ng, N., H. Kroll, J., W. H. Chan, A., S. Chhabra, P., C. Flagan, R., & H. Seinfeld, J. (2007, July). Secondary organic aerosol formation from m -xylene, toluene, and benzene. *Atmos. Chem. Phys.*, *7*.

Ortiz-Montalvo, D. L., Häkkinen, S. A. K., Schwier, A. N., Lim, Y. B., McNeill, V. F., & Turpin, B. J. (2014, January). Ammonium Addition (and Aerosol pH) Has a Dramatic Impact on the Volatility and Yield of Glyoxal Secondary Organic Aerosol. *Environ. Sci. Technol.*, *48*(1), 255–262.

Sareen, N., Carlton, A. G., Surratt, J. D., Gold, A., Lee, B., Lopez-Hilfiker, F. D., … Turpin, B. J. (2016, November). Identifying precursors and aqueous organic aerosol formation pathways during the SOAS campaign. *Atmos. Chem. Phys.*, *16*(22), 14409–14420.

Schnitzhofer, R., Metzger, A., Breitenlechner, M., Jud, W., Heinritzi, M., De Menezes, L.-P., … Hansel (2014, July). Characterisation of organic contaminants in the CLOUD chamber at CERN. *Atmospheric Measurement Techniques*, *7*.

Shrivastava, M., Cappa, C. D., Fan, J., Goldstein, A. H., Guenther, A. B., Jimenez, J. L., … Zhang, Q. (2017). Recent advances in understanding secondary organic aerosol: Implications for global climate forcing. *Reviews of Geophysics*, *55*(2), 509–559.

Sörgel, M., Regelin, E., Bozem, H., Diesch, J.-M., Drewnick, F., Fischer, H., … Zetzsch, C. (2011, October). Quantification of the unknown HONO daytime source and its relation to NO2. *Atmos. Chem. Phys.*, *11*.

Spracklen, D. V., Jimenez, J. L., Carslaw, K. S., Worsnop, D. R., Evans, M. J., Mann, G. W., … Forster, P. (2011). Aerosol mass spectrometer constraint on the global secondary organic aerosol budget. *Atmospheric Chemistry and Physics*, *11*(23), 12109–12136.

Stubenrauch, C. J., Rossow, W. B., Kinne, S., Ackerman, S., Cesana, G., Chepfer, H., … Zhao, G. (2013, January). Assessment of Global Cloud Datasets from Satellites: Project and Database Initiated by the GEWEX Radiation Panel. *Bull. Amer. Meteor. Soc.*, *94*(7), 1031–1049.

Stutz J., Kim E. S., Platt U., Bruno P., Perrino C., & Febo A. (2000, June). Uv-visible absorption cross sections of nitrous acid. *Journal of Geophysical Research: Atmospheres*, *105*(D11), 14585–14592.

Tadić, J., Moortgat, J., & Wirtz, K. (2006). Photolysis of glyoxal in air. *Journal of Photochemistry and Photobiology Chemistry*.

Tan, Y., Perri, M. J., Seitzinger, S. P., & Turpin, B. J. (2009, November). Effects of Precursor Concentration and Acidic Sulfate in Aqueous Glyoxal-OH Radical Oxidation and Implications for Secondary Organic Aerosol. *Environ. Sci. Technol.*, *43*(21), 8105–8112.

Tanner, J. P., Salemi, J. L., Stuart, A. L., Yu, H., Jordan, M. M., DuClos, C., … Kirby, R. S. (2015, October). Associations between exposure to ambient benzene and PM2.5 during pregnancy and the risk of selected birth defects in offspring. *Environmental Research*, *142*, 345–353.

Teng, C., Wang, Z., & Yan, B. (2016). Fine particle-induced birth defects: Impacts of size, payload, and beyond. *Birth Defects Research Part C: Embryo Today: Reviews*, *108*(3), 196–206.

Thurston, G., Ahn, J., Cromar, K., Shao, Y., Reynolds, H., Jerrett, M., … Hayes, R. (2015, January). Ambient particulate matter air pollution exposure and mortality in the NIH-AARP diet and health cohort. *Environmental Health Perspectives*, *124*.

van den Hooven, E. H., de Kluizenaar, Y., Pierik, F. H., Hofman, A., van Ratingen, S. W., Zandveld, P. Y., … Jaddoe, V. W. (2012, May). Chronic Air Pollution Exposure during

Pregnancy and Maternal and Fetal C-Reactive Protein Levels: The Generation R Study. *Environmental Health Perspectives*, *120*(5), 746–751.

Volkamer, R., SanMartini, F., Molina, L. T., Salcedo, D., Jimenez, J. L., & Molina, M. J. (2007, October). A missing sink for gas-phase glyoxal in Mexico City: Formation of secondary organic aerosol. *Geophysical Research Letters*, *34*(19).

Volkamer, R., Sheehy, P., Molina, L. T., & Molina, M. J. (2010, July). Oxidative capacity of the Mexico City atmosphere - Part 1: A radical source perspective. *Atmos. Chem. Phys.*, *10*(14), 6969–6991.

Volkamer, R., Ziemann, J., & Molina, M. (2009, March). Secondary Organic Aerosol Formation from Acetylene (C2h2): Seed effect on SOA yields due to organic photochemistry in the aerosol aqueous phase. *Atmospheric Chemistry and Physics*, *9*.

Wang, J., Doussin, J., Perrier, S., Perraudin, E., Katrib, Y., Pangui, E., & Picquet-Varrault, B. (2011). Design of a new multi-phase experimental simulation chamber for atmospheric photosmog, aerosol and cloud chemistry research. *Atmospheric Measurement Techniques*, *4*(11), 2465.

Yaping, X., Daniel, J., & Solene, T. (2007, June). Atmospheric acetylene and its relationship with CO as an indicator of air mass age. *Journal of Geophysical Research: Atmospheres*, *112*(D12).

Yeung, L. Y., Pennino, M. J., Miller, A. M., & Elrod, M. J. (2005, March). Kinetics and Mechanistic Studies of the Atmospheric Oxidation of Alkynes. *J. Phys. Chem. A*, *109*(9), 1879–1889.

Zhang, Q., L. Jimenez, J., R. Canagaratna, M., D. Allan, J., Coe, H., Ulbrich, I., … Worsnop, D. (2013, April). Ubiquity and dominance of oxygenated species in organic aerosols in anthropogenically-influenced Northern Hemisphere midlatitudes. *Geophysical Research Letters*, *34*.